Eurasian Journal of Physics and Functional Materials

Volume 8 | Number 3

Article 7

Pages: 155 - 161

2024

Investigation of thermal and electrical properties of composite cathode materials Pr1−xSrxFe1−yCoyO3 (x= 0.3,0.4; y = 0.2): GDC and La2Ni1-xCoxO4+δ (x= 0.2): GDC for SOFC

Bekmyrza K.Zh.
Faculty of Physics and Technical Sciences, L.N. Gumilyov Eurasian National University, Astana 010008, Kazakhstan

Bakalbayeva G.A.
Faculty of Physics and Technical Sciences, L.N. Gumilyov Eurasian National University, Astana 010008, Kazakhstan

Kabyshev A.M.
Faculty of Physics and Technical Sciences, L.N. Gumilyov Eurasian National University, Astana 010008, Kazakhstan, assetenu@gmail.com

Aidarbekov N.K.
Faculty of Physics and Technical Sciences, L.N. Gumilyov Eurasian National University, Astana 010008, Kazakhstan

Baratova A.A.
Faculty of Physics and Technical Sciences, L.N. Gumilyov Eurasian National University, Astana 010008, Kazakhstan

Investigation of thermal and electrical properties of composite cathode materials Pr1−xSrxFe1−yCoyO3 (x= 0.3,0.4; y = 0.2): GDC and La2Ni1-xCoxO4+δ (x= 0.2): GDC for SOFC

Authors

Bekmyrza K.Zh., Bakalbayeva G.A., Kabyshev A.M., Aidarbekov N.K., Baratova A.A., Kubenova M.M., Kabdrakhimova G.D., and Kuterbekov K.A.

ORIGINAL STUDY

Investigation of Thermal and Electrical Properties of Composite Cathode Materials $Pr_{1-x}Sr_xFe_{1-y}Co_yO_3$ (x = 0.3, 0.4; y = 0.2): GDC and $La_2Ni_{1-x}Co_xO_{4+\delta}$ (x = 0.2): GDC for SOFC

Kenzhebatyr Zh. Bekmyrza*, Gulshat A. Bakalbayeva, Asset M. Kabyshev, Nursultan K. Aidarbekov, Aliya A. Baratova, Marzhan M. Kubenova, Gaukhar D. Kabdrakhimova, Kairat A. Kuterbekov

Faculty of Physics and Technical Sciences, L.N. Gumilyov Eurasian National University, Astana 010008, Kazakhstan

Abstract

The electrical and thermal properties of composite cathode materials $Pr_{1-x}Sr_xFe_{1-y}Co_yO_3$ (x = 0.3, 0.4; y = 0.2): GDC and $La_2Ni_{1-x}Co_xO_{4+\delta}$ (x = 0.2):GDC for solid oxide fuel cells (SOFC) were investigated. As the second component of the composites, GDC electrolyte was chosen. The reason for this choice is that GDC has greater chemical inertness in relation to cathode materials compared to YSZ. Additionally, GDC is characterized by higher ionic conductivity, which makes it preferable for use in composites. The sintering kinetics of composite materials differs significantly from that of pure cathode materials, with the sintering temperature being several degrees lower for composite materials.

Keywords: SOFC, Composite cathode materials, Coefficients of thermal expansion, Conductivity

1. Introduction

Perovskite-structured materials (ABO3) are one of the most common families of complex oxides. The presence of various A- and B-cations in the perovskite structure, differing in their crystallochemical characteristics, allows for significant changes in the chemical composition of the phase and, consequently, allows for targeted manipulation of its properties. Moreover, the properties of perovskite-type materials can be significantly influenced by doping with A- and/or B-cations, as well as by the ordering effects of ions and the level of oxygen nonstoichiometry.

Detailed reviews of perovskite and perovskite-like structures are presented in works [1–8]. This section provides a brief description of these structures to clearly delineate the differences between them.

The ideal cubic structure of perovskite ABO_3 (space group $Pm\bar{3}m$) is shown in Fig. 1 [4]. B cations are located at the corners, while A cations are in the center of the unit cell. Anions (oxygen ions) are positioned at the centers of the twelve cubic faces, forming the vertices of the octahedra BO6. The coordination numbers of A and B cations are 12 and 6, respectively. The radius of the A ion is close to that of the anion, so large low-charge ions from alkali, alkaline earth, and rare earth metals can serve as A cations. Transition metal ions of medium size typically act as B cations.

Few compounds are characterized by a perfect cubic structure. In most cases, oxides have a slightly distorted version of the structure with lower symmetry (for example, hexagonal or orthorhombic). The deviation from the ideal structure in perovskite oxides can be assessed using the tolerance factor (t), which was first applied by Goldschmidt in 1926 [9]:

$$t = \frac{r_A + r_O}{\sqrt{2}(r_B + r_O)}, \quad (1)$$

Received 10 September 2024; revised 15 September 2024; accepted 18 September 2024.
Available online 19 October 2024

* Corresponding author.
E-mail address: assetenu@gmail.com (A.M. Kabyshev).

https://doi.org/10.69912/2616-8537.1230

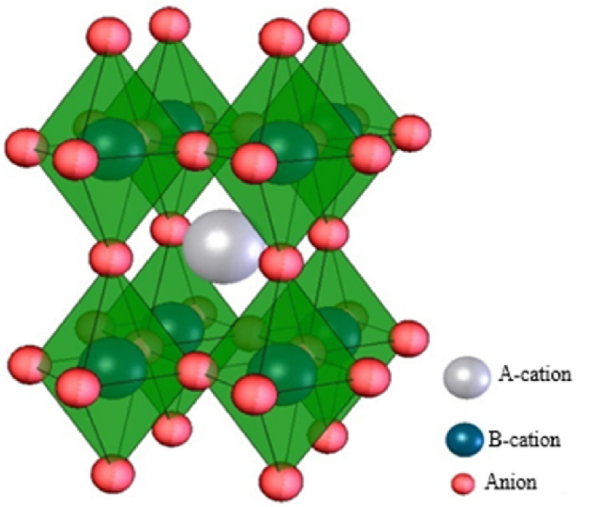

Fig. 1. Structure of cubic perovskite ABO_3.

where r_A, r_B, and r_O are the ionic radii of the A-site cations, B-site cations, and anions, respectively.

In a perfect cubic perovskite structure, t should be equal to 1.0. Empirically, it has been found that generally, the cubic structure of perovskite is maintained when t is in the range of 0.9–1.0. When $t > 1$, which can happen due to a larger radius of the A-cation or a smaller radius of the B-cation, hexagonal variants of the perovskite structure, such as $BaNiO_3$ types, will be stable. In cases where $0.9 > t > 0.71$, the BO_6 octahedra tilt to fill the cuboctahedral coordination polyhedron, leading to a reduction in the crystal symmetry [10–13]. At lower t values, where the A- and B-cations have similar radii, the perovskite structure degenerates into an ilmenite structure [14–16].

The degree of distortion of the perovskite structure, which affects the material's properties, can be altered by partially substituting A- and/or B-cations ($A_{1-x}A'_xBO_3$, $AB_{1-x}B'_xO_3$ и $A_{1-x}A'_xB_{1-y}B'_yO_3$). For example, most un-doped perovskite materials have low oxygen ion conductivity in air. When the A-cation (or B-cation) is partially replaced with acceptor cations, it leads to the formation of oxygen vacancies and, consequently, an increase in ionic conductivity. However, in some cases, when the charges or ionic radii of the host and dopant cations differ significantly, lattice energy can be reduced by ordering some or all types of ions into available crystallographic positions. This process results in the formation of double perovskites.

1.1. Double perovskites

Doping is a very common method for modifying the properties of perovskite compounds. Both A- and B-cations can be partially replaced to varying degrees. However, when exactly half of the A- or B-cations are replaced by another cation, structural ordering can occur. This leads to the formation of so-called double perovskites. Their general formula can be written as $A_{0.5}A'_{0.5}BO_{3-\delta}$ (or $AB_{0.5}B'_{0.5}O_{3-\delta}$). However, when there's a significant difference in the radii of the host cations and the dopant, the structure tends to become ordered, and the material's formula is usually written as $AA'B_2O_{5+\delta}$ (or $A_2BB'O_{5+\delta}$). A detailed description of the double perovskites $A_2BB'O_6$ is provided in Ref. [4].

The literature describes three simple types of ordering of A- or B-cations in the perovskite structure (Fig. 2).

The most symmetrical ordering is that of the type found in rock salt, since the arrangement of A- and A′-cations (or B and B′-cations) is equivalent to the positioning of the anion and cation in the rock salt structure. Additionally, in an ordered state, cations can form columnar and layered structures. Generally, B-cations tend to create ordered structures more « easily » than A-cations.

When it comes to ordering B/B′-cations in $A_2BB'O_6$ perovskites, rock salt-type ordering is most common, whereas for A/A′-cations in $AA'B_2O_6$ and $AA'BB'O_6$ perovskites, layered ordering is the most likely scenario. The reasons and conditions for all types of ordering in perovskite structures are described in detail in work [3].

The influence of structure on the properties of cathode materials. Electrical conductivity.

The nature of electronic conductivity is similar across all perovskite-like structures. It is believed that the B-O-B bond is primarily responsible for the electrical properties of these compounds [17]. The BO_6 octahedra create a network throughout the perovskite structure, and electronic conductivity occurs due to the transfer

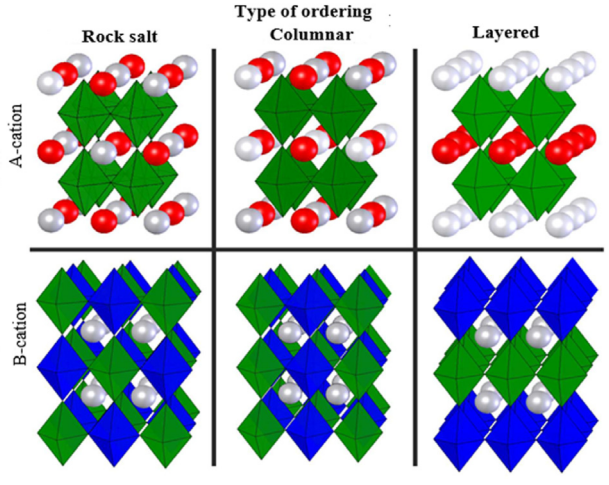

Fig. 2. Cation ordering schemes in perovskites. From left to right, the arrangements are shown for rock-salt type, columnar, and layered for A-cations in the compositions $AA'B_2O_6$ (top) and B-cations in $A_2BB'O_6$ (bottom).

of electrons or holes along the B-O-B bonds. The interaction between the B cation's d-orbitals and the oxygen ion's p-orbitals leads to electron-hole exchange (see Fig. 3). Thus, perovskite oxides containing transition metals with incompletely filled d-orbitals as the B cation can exhibit high electrical conductivity. In the case of the cubic perovskite structure, the overlap of orbitals is most efficient, while the degree of overlap decreases with distortion of the perovskite structure, leading to reduced conductivity. Therefore, considering the aforementioned tolerance factor *t*, among ABO_3 perovskites, the highest electronic conductivity should be observed for compounds with larger A cations, such as La and Pr [1].

Moreover, according to the aforementioned dual exchange mechanism, for achieving high electronic conductivity, it is necessary for the B-cation to have an incompletely filled d-shell, meaning it must be able to change its oxidation state [1,18]. Electronic conductivity can be n-type or p-type, depending on the material properties and the partial pressure of surrounding oxygen. n-type electronic conductors are usually unstable at high temperatures in air or other oxidizing atmospheres because generating electrons requires oxygen non-stoichiometry. On the other hand, p-type electronic conductors are typically stable in air, as generating holes requires an excess of oxygen [19]. Thus, the most preferred candidates for B-cation are Cr, Mn, Fe, Co, and Ni [1]. In this case, cobalt-, manganese-, and nickel-containing oxides exhibit the highest electronic conductivity.

Moreover, the electrical conductivity of perovskite can change with partial substitution (doping) of A- and/or B-cations. In isovalent substitution, the doping ions (A′ and/or B′) affect the electronic conductivity due to ionic radii. Smaller ions lead to distortion of the perovskite structure, and consequently, a reduction in its electronic conductivity. In heterovalent substitution of the A-cation, where the ions differ in both valency and radii, the relationship is more complex. To maintain the crystal's electroneutrality, the valency change resulting from the doping of the A-cation must be balanced either by a change in the valency of the B-cation (the transition metal) or by creating vacancies in the oxygen sublattice. In this case, the radius of the transition metal also depends on its valency state. Thus, introducing dopants distorts the lattice on one hand while increasing the concentration of charge carriers (holes) on the other. It's preferable for the dopants to have an ionic radius close to that of the host cation. For instance, it is known that substituting La3+ with alkaline earth metal ions Ca^{2+}, Sr^{2+}, and Ba^{2+} enhances electronic conductivity. It should be noted that the reactivity of the oxides of alkaline earth metals increases as you go from calcium to barium. Thus, a drawback of barium-containing perovskites is their chemical interaction with electrolytes and CO_2 present in the air.

From comparing the electronic conductivity data, it's clear that La-Co-based compounds with an unordered cubic structure have the highest electronic conductivity, while the conductivity of the ordered perovskites and Ruddlesden-Popper phases is significantly lower. I'd also like to point out a detailed review [20], which gathers data on the conductivity of a huge number of perovskite compounds with a layered structure.

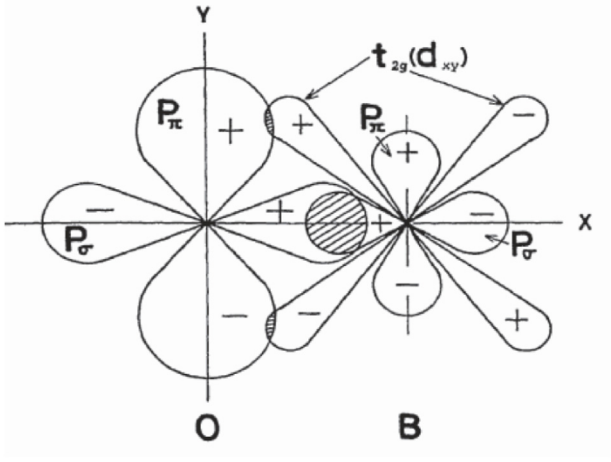

Fig. 3. Covalent bonds between the p-orbitals of the oxygen ion and the d-orbitals of the B-cation [17].

2. Experimental

2.1. Synthesis of selected compositions

When creating composite cathodes, materials with high Co content (LNC-30 and PSFC-3050) were excluded due to their high chemical reactivity with the YSZ and GDC electrolytes and their high polarization resistance. The compositions LNC-10, PFC-20, PSFC-1020, and PSFC-2020 were set aside because of their low conductivity and high polarization resistances (except for PSFC-2020). Therefore, the following cathode materials were selected for the composites: La_2NiO_4, $La_2Ni_{0.8}Co_{0.2}O_4$, Pr_2NiO_4, $Pr_{0.7}Sr_{0.3}Fe_{0.8}Co_{0.2}O_3$, and $Pr_{0.6}Sr_{0.4}Fe_{0.8}Co_{0.2}O_3$. It should be noted that the PN composition, which has the lowest polarization resistance and the highest conductivity among the studied materials with the Ruddlesden-Popper structure, nevertheless exhibits high chemical activity towards the electrolytes (even towards GDC).

As a second component of the composites, the electrolyte GDC was chosen. This material is more chemically inert with respect to cathode materials than YSZ and also has higher ionic conductivity. One composite

was made with the electrolyte YSZ and the cathode material PSFC-4020 to evaluate the effect of the electrolyte's nature on the thermal properties of the composites.

The preparation of composite mixtures was carried out according to the following method. The mixture of powders with the specified ratio of components was poured with isopropyl alcohol and subjected to ultrasonic treatment to eliminate the agglomeration of nanosized electrolyte powders. The treatment was performed using a disperser for 15 min. Further mixing of the powders was done with a gravity mixer for at least 2 days. YSZ balls were added to the suspensions as milling media. The drying of the resulting mixtures was carried out with constant stirring using a magnetic stirrer RH B S000 (IKA).

The original nanoscale powder of the electrolyte material $Zr_{0.84}Y_{0.16}O_{2-\delta}$ (YSZ) was obtained by laser evaporation in Ref. [21]. A commercial powder of $Ce_{0.9}Gd_{0.1}O_{2-\delta}$ (GDC) produced by Kceracell Co., Ltd. was used as the electrolyte based on CeO_2.

To increase the particle size and thereby change the kinetics of the electrolytes' sintering, the starting powders were sintered at various temperatures ranging from 800 to 1100 °C. The holding time at the sintering temperature was 4 h in all experiments. The sintered powders will be denoted as: composition-Ts, where Ts is the sintering temperature in °C. For example, YSZ-1000 denotes that the YSZ powder was sintered at 1000 °C.

The powder of the cathode material $La_{0.7}Sr_{0.3}MnO_3$ (LSM) was obtained by pyrolyzing a polymer-salt composition (polyvinyl alcohol and nitrates) [22]. The starting reagents were $La(NO_3)_3$ (analytical grade), $Sr(NO_3)_2$ (chemically pure), and $Mn(NO_3)_2$ (analytical grade). The stoichiometric mixture of the reagents was dissolved in distilled water with the addition of polyvinyl alcohol (grade 11/2) in a polymer/salt ratio of 2. The resulting solution was heated in a porcelain cup to remove water and initiate the pyrolysis of the polyvinyl alcohol. In the final stage of the synthesis, the reaction mixture was annealed at 1100 °C for 10 h.

The other cathode materials were made using a self-propagating high-temperature synthesis method. The synthesis process was based on a variant of the Pechini method described in Ref. [23]. The reagents used were $Pr(NO_3)_3$ (analytical grade), $Fe(NO_3)_3$ (analytical grade), $Co(NO_3)_2$ (chemically pure), La_2O_3 (chemically pure), NiO (analytical grade), and $SrCO_3$ (analytical grade). Stoichiometric mixtures of the reagents were dissolved in a 0.1 N HNO_3 solution until a homogeneous solution was obtained, which was then evaporated to wet salts. Ethylene glycol $HOCH_2CH_2OH$ (chemically pure) was used as the combustible organic substance, which acted as both a solvent and a reagent. The reaction mixture was heated until the self-propagating high-temperature synthesis process began. The reaction products were regrinded and then subjected to staged calcination to remove residues of the organic phase at temperatures of 400, 700, and 900 °C, holding for 6 h at each temperature. The final stage of treatment was calcination at 1100 °C for 30 min.

2.2. Kinetics of sintering and thermal expansion of composite cathodes

For cathode materials used in solid oxide fuel cells (SOFC), thermal expansion is an important physical property. Differences in the coefficients of thermal expansion (CTE) between components can lead to damage in the fuel cell.

The sintering kinetics of composite materials were studied on samples in the form of discs with a diameter of 8 mm and a thickness of ~3 mm, pressed to a relative density of ~0.5−0.7. The linear expansion of the composites was measured on samples in the form of bars with typical dimensions of (4 × 4 × 9.5) mm, which were pre-sintered to densities close to theoretical values. The sintering regime (1250 °C, with a 7-h hold) was selected based on the results of the sintering kinetics study. In both cases, the samples were pressed using a uniaxial hydraulic press.

The sintering kinetics and linear expansion of the materials were investigated in an air atmosphere over temperature ranges of 20−1300 °C and 20−1200 °C, respectively. The measurements were carried out using a Dil 402C dilatometer. The heating rate was 5 °C/min.

2.3. Conductivity investigation

For conductivity measurements, the composite mixtures were pressed into rectangular bars with dimensions 3 × 2 × 30 mm. The samples were compacted using a press and then sintered in an air atmosphere at 1250 °C.

Platinum wire probes with a diameter of 0.2 mm were attached to the sintered samples. To ensure reliable electrical contact, the probes were coated with platinum paste, which was then sintered at 1000 °C for 1 h.

Conductivity measurements were performed in air using the four-point probe method with direct current over a temperature range of 20−850 °C, employing a Solartron SL-1260/1287 impedance analyzer.

3. Results and discussion

The sintering kinetics of composite materials differ significantly from those of pure cathode materials. Fig. 4 illustrates the results of the sintering kinetics

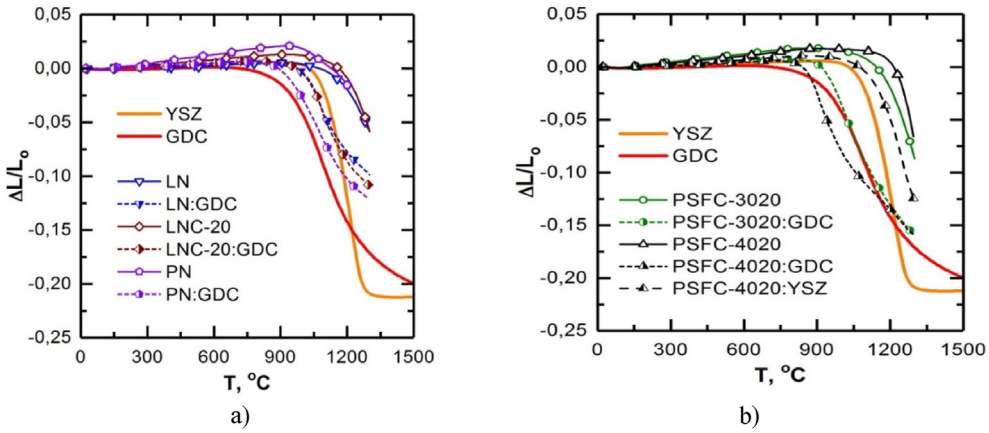

Fig. 4. Linear shrinkage curves of composite samples based on cathode materials: (a) with Ruddlesden-Popper structure, (b) with perovskite structure.

study for composite cathode materials. The data indicate that the sintering kinetics of composites is substantially different from that of pure cathode materials. The onset of sintering for the composites occurs 300–400 °C lower than that for pure cathodes. Additionally, the shape of the sintering curve has changed: in the high-temperature range, the sintering process slows down, which is likely related to the influence of GDC.

The formation of the composite had a lesser impact on the sintering of materials with a Ruddlesden-Popper structure compared to PSFC materials. The sintering curves of composites LN:GDC, LNC-20:GDC, and PN:GDC can be viewed as a superposition of the sintering curves of the respective pure cathode materials and the GDC electrolyte. In contrast, the sintering curve of the PSFC-3020:GDC composite closely matches the GDC sintering curve, while the sintering curve of PSFC-4020:GDC is even lower than the GDC curve. This behavior is likely related more to the morphology of the initial powders rather than the chemical nature of the cathode materials. The perovskite cathode powders PSFC-3020 and PSFC-4020, in addition to large particles of 1–3 μm, contain a significant amount of small rounded particles smaller than 0.4 μm, whereas the powders LN, LNC-20, and PN do not have a fine particle fraction.

Fig. 5 shows the results of linear expansion measurements of composite cathode materials over the temperature range (20–1200)°C. The average coefficients of thermal expansion (CTE) for the corresponding temperature ranges are summarized in Table 1.

Fig. 6 shows the temperature dependence of conductivity for composite materials compared to data for pure cathode materials and the GDC electrolyte.

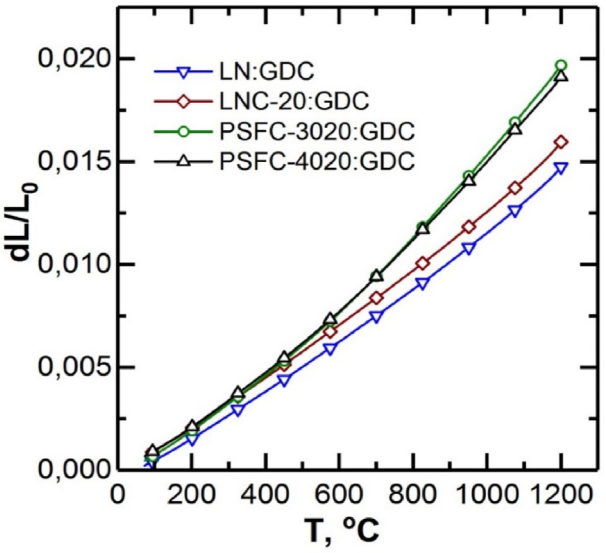

Fig. 5. Temperature dependence of dimensional changes in composite cathode material samples.

Table 1. Coefficients of thermal expansion (CTE) of composite cathode materials.

Composite	Temperature Range, (°C)	CTE ($\times 10^{-6}$), K^{-1}
Composite Cathode Materials		
LN:GDC	200–850	12.91
	850–1200	14.84
LNC-20:GDC	200–850	12.84
	850–1200	15.59
PSFC-3020:GDC	200–700	14.83
	700–1200	20.40
PSFC-4020:GDC	300–800	15.51
	800–1200	19.67
Electrolytes		
YSZ	200–1000	10.9
GDC	200–1000	13.1

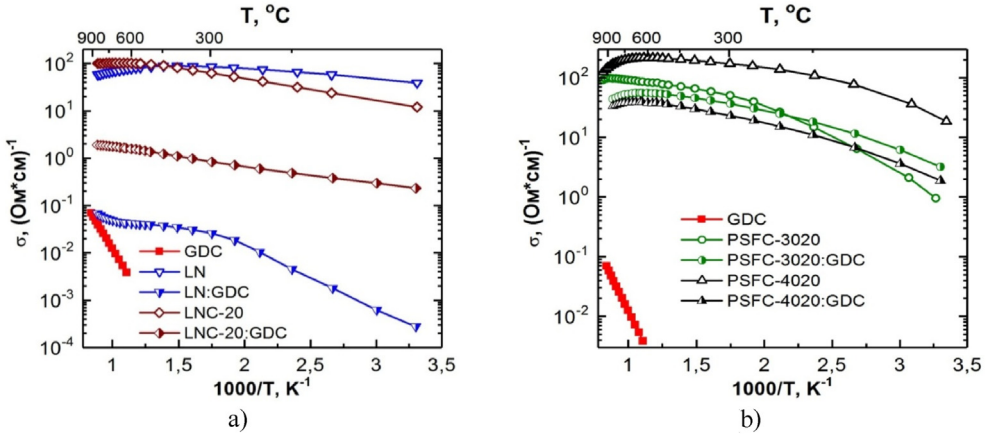

Fig. 6. Temperature dependence of conductivity for composite cathode materials: (a) with Ruddlesden-Popper structure, (b) with Perovskite structure.

The data indicate that the conductivity of composites based on Ruddlesden-Popper structure materials differs significantly from that of pure cathode materials. For instance, the conductivity of the LNC-20:GDC composite decreased by two orders of magnitude compared to pure LNC-20, and the conductivity of the LN:GDC composite decreased by three orders of magnitude, approaching the conductivity of GDC at high temperatures. In contrast, the reduction in conductivity for composites based on praseodymium ferro-cobaltite was less pronounced. At 800 °C, the conductivity of the PSFC-4020:GDC composite decreased by a factor of 5 compared to PSFC-4020, while the conductivity of PSFC-3020:GDC decreased only by a factor of 2 relative to PSFC-3020.

4. Conclusion

The obtained data confirm the intuitive assumption that the coefficient of thermal expansion (CTE) of a composite material should be an intermediate value between the CTEs of its components. Thus, the creation of composite materials brings the CTE values of the electrolyte and the cathode layer closer together. This, in turn, can reduce mechanical stresses in the non-porous cathode-electrolyte structure, helping to prevent material delamination during operation and thermal cycling.

Funding

This research was funded by the grant with reference number BR21882359, provided by the Ministry of Science and Higher Education of Kazakhstan.

Conflict of interest

The authors have no conflicts of interest to declare that are relevant to the content of this article.

References

[1] С.Я. ИстоМин, Е.В. Антипов, Катодные Материалы на основе перовскитоподобных оксидов переходных Металлов для среднетеМпературных твердооксидных топливных элеМентов, Успехи хиМии 82 (2013) 686–700.
[2] A.S. Bhalla, R. Guo, R. Roy, The perovskite structure – a review of its role in ceramic science and technology, Mater. Res. Innovat. 4 (2000) 3–26.
[3] G. King, P.M. Woodward, Cation ordering in perovskites, J. Mater. Chem. 20 (2010) 5785–5796.
[4] S. Vasala, M. Karppinen, $A_2B'B''O_6$ perovskites: a review, Prog. Solid State Chem 43 (2015) 1–36.
[5] B.V. Beznosikov, K.S. Aleksandrov, Perovskite-like crystals of the ruddlesden–popper series, Crystallogr. Rep. 45 (2000) 792–798.
[6] A.M. Abakumov, M.G. Rozova, et al., Complex manganese oxides with the brownmillerite structure: synthesis, crystal chemistry and properties, Russ. Chem. Rev. 73 (2004) 847–860.
[7] J. Young, J.M. Rondinelli, Crystal structure and electronic properties of bulk and thin film brownmillerite oxides, Phys. Rev. B 92 (17) (2015) 1–10.
[8] A.V. Nikonov, R.A. Kuterbekov, K.Zh. Bekmyrza, et al., A brief review of conductivity and thermal expansion of perovskite-related oxides for SOFC cathode, Eurasian J. Phys. Funct. Mater. 2 (2018) 274–292.
[9] V.M. Goldschmidt, Die Gesetze der Krystallochemie, Naturwissenschaften 14 (1926) 477–485.
[10] A.M. Glazer, The classification of tilted octahedra in perovskites, Acta Crystallogr. B28 (1972) 3384–3392.
[11] P.M. Woodward, Octahedral tilting in perovskites. I. Geometrical considerations, Acta Crystallogr. B53 (1997) 32–43.
[12] C.J. Howard, H.T. Stokes, Group-theoretical analysis of octahedral tilting in perovskites, Acta Crystallogr. B54 (1998) 782–789.
[13] R.J.D. Tilley, Perovskites. Structure–Property Relationships, John Wiley & Sons Ltd. UK, Hoboken, NJ, 2016, p. 315.
[14] S.N. Ruddlesden, P. Popper, The compound $Sr_3Ti_2O_7$ and its structure, Acta Crystallogr. B 11 (1958) 54–55.
[15] A.V. Nikonov, N.B. Pavzderin, V.R. Khrustov, I.V. Semenova, K.I. Demidova, K.A. Kuterbekov, K.Zh. Bekmyrza, S.N. Nurakov, T.A. Koketay, O.I. Gyrdasova, Investigation of thermal, electrical, and electrochemical properties of Pr1−xSrxFe1−yCoyO3 ($0 < x < 0.4$; $y = 0.2, 0.5$) cathode materials for SOFC // Journal of Alloys and Compounds, RSC Adv. 865 (5 June 2021) 158898, https://doi.org/10.1016/j.jallcom.2021, 158898.
[16] Lukman Ahmed Omeiza, Asset Kabyshev, Kenzhebatyr Bekmyrza, Kairat A. Kuterbekov, Marzhan Kubenova, Zhuldyz A. Zhumadilova, Yathavan Subramanian, Muhammed Ali, Nursultan Aidarbekov, Abul Kalam Azad, Constraints in sustainable electrode materials

development for solid oxide fuel cell: A brief review, Materials Science for Energy Technologies 8 (2025) 32—43, https://doi.org/10.1016/j.mset.2024.07.001.
[17] J. Sunarso, S.S. Hashim, et al., Perovskite oxides applications in high temperature oxygen separation, solid oxide fuel cell and membrane reactor: a review, Prog. Energy Combust. Sci. 61 (2017) 57—77.
[18] H. Kozuka, K. Ohbayashi, et al., Electronic conduction in La-based perovskite-type oxides, Sci. Technol. Adv. Mater. 16 (2015) 2—11.
[19] R. Pelosato, G. Cordaro, et al., Cobalt based layered perovskites as cathode material for intermediate temperature Solid Oxide Fuel Cells: a brief review, J. Power Sources 298 (2015) 46—67.
[20] D.Z. de Florio, F.C. Fonseca, et al., Ceramic materials for fuel cells, Cerâmica 50 (2004) 275—290.
[21] M. Ivanov, V. Osipov, et al., Laser synthesis of oxide nanopowders, Adv. Sci. Technol. 45 (2006) 291—296.
[22] А.А. Остроушко, А.Е. Удилов, Некоторые особенности процессов форМирования слоЖнооксидных продуктов МетодоМ пиролиза полиМерно-солевых коМпозиций, ХиМия и ХиМическая Технология 50 (2007) 118—123.
[23] Т.И. Чупахина, О.И. Gырдасова, G.B. Базуев, Синтез, структурные и Морфологические характеристики ультрадисперсных порошков и кераМики на основе твердых растворов La2-xSr0.125PrxNiO4 (0≤ x≤1.775), Известия РАН 77 (2013) 1276—1280.